CARBON 67 (2014) 304–317

Available at www.sciencedirect.com

ScienceDirect

journal homepage: www.elsevier.com/locate/carbon

Post-modification by low-temperature annealing of carbon nano-onions in the presence of carbohydrates

Marta E. Plonska-Brzezinska [a,*], *Agustin Molina-Ontoria* [b], *Luis Echegoyen* [b]

[a] *Institute of Chemistry, University of Bialystok, Hurtowa 1, 15-399 Bialystok, Poland*
[b] *Department of Chemistry, University of Texas at El Paso, 500 W. University Ave., El Paso, TX 79968, USA*

ARTICLE INFO

Article history:
Received 16 March 2013
Accepted 24 September 2013
Available online 8 October 2013

ABSTRACT

The structural and electrochemical properties of carbon nano-onions (CNOs) were investigated in the solid phase, for both plain as well as post-modified CNOs in the absence/presence of carbohydrates (glucose or starch) in an air atmosphere. The structural properties of the CNOs were changed as a consequence of the post-modification during low-temperature annealing. This process changes the carbon structures into predominantly higher ordered graphitic layers.

TEM studies clearly showed that polygonization of the CNOs occurred during the annealing process, corresponding to the creation of some of diamond-like structures with predominantly spherical-CNO and ribbon-like graphite structures. Additional graphitization led to an increase of the BET specific surface area, and reached a maximum of 511 $m^2 g^{-1}$ for the post-modified CNOs/starch material. According to the pore size distribution curves of the BJH adsorption, we estimated the pore diameter sizes mainly between the 2 and 50 nm diameter.

The electrochemical properties of the CNO films depend on the porous structures of the carbon surface. In aqueous solutions, all CNO films show the typical behavior of an ideal double layer capacitor. The voltammetric behavior of CNO films depends on the counterions.

1. Introduction

Carbon-based nanomaterials, such as fullerenes, single- and multi-walled carbon nanotubes, carbon nanofibers, nano-onions or graphene, are currently some of the most interesting and potential useful nanostructures. Unique mechanical, chemical, thermal, optical or electrical behavior of these nanomaterials are related to their shape, size, and surface area, and these provide many application possibilities. Therefore, carbon-based nanomaterials have been used in microelectronic and optoelectronic devices [1], as energy storage materials [2], and electrocatalysts [3], and in polymer composites [4–7]. The physical properties of the carbon materials must be controlled for optimal electrochemical performance, especially their surface area, pore volume, and pore size. Carbon-based electrochemical capacitors (ECs), also called electrical double layer capacitors (EDLCs) [8], store energy at the electrolyte–carbon interface through reversible ion adsorption onto the carbon surface. The capacitance can be described according to [8]:

* *Corresponding author:* Fax: +48 85 747 0113.
E-mail address: mplonska@uwb.edu.pl (M.E. Plonska-Brzezinska).
0008-6223/$ - see front matter
http://dx.doi.org/10.1016/j.carbon.2013.09.093

$$C = \frac{\varepsilon_r \varepsilon_0 A}{d} \quad (1)$$

where ε_r is the electrolyte dielectric constant, ε_0 is the permittivity of a vacuum, A the surface area accessible to the ions and d the distance between the center of the ion and the carbon surface. The charge in EDLCs is stored only on the surface of the carbon. The electric charge is accumulated on the electric double-layers on the polarized electrodes, thus electrodes with higher surface area can store more energy. The low energy density of EDLCs has limited their applications. A systematic study of the effects of carbon microstructures, with different macro-, micro-, and meso-porous outer surfaces, on ion-electrode interactions, has been performed by Simon et al. using nanoporous carbons [9,10].

Carbon nano-onions (CNOs) are spherical structures first produced by irradiation of nanoparticles under an electron beam by Ugarte in 1992 [11]. The first time onion-like structures were observed in 1980 by Iijima et al. in amorphous carbon films prepared by a vacuum evaporation method [12]. Carbon nano-onions consist of a multilayered arrangement of closed fullerene shells. The distance between the layers is very close to the interlayer distance in bulk graphite (0.335 nm) [13]. Although various methods have been published for the synthesis of carbon nano-onions, most of these methods lead to CNOs with a large number of shells and generally result in low yields [14,15]. The method developed by Kuznetsov et al. [16] is based on temperature annealing of ultradispersed nanodiamond (ND) particles of about 5 nm in average diameter and results in gram quantities of CNOs with very high purity and narrow size dispersity. The resulting CNOs consist of a few shells while their sizes are somewhat larger than those of the ND precursors, because of the lower density of graphitic carbon [17]. Generally, carbon nano-onions exhibit low density and large surface to volume ratios [11]. Recent studies of onion-like structures show high conductivity similar to that of carbon black (~4S cm^{-1}) and graphitic structures that are attractive for many applications [18,19]. Therefore, CNOs have potential applications in supercapacitor electrodes [4–7,20], as cathodes in Li–ion electrochemical energy storage devices [21], as optical limiting agents [22], and as electron field emitters [23,24].

Experimental [25] and theoretical [26,27] evidence clearly show that CNOs obtained from ultradispersed diamond nanoparticles could have different graphene-like structures: spherical, spheroidal or ellipsoidal, with various phases. The applications of CNOs are in most cases based on the diverse properties of various phases including onion-like carbon, nanodiamonds, and bucky-diamond (diamond-like core and single/multiple graphitic cage-like shells) [28–32]. Structural-modification of the multi-layered spherical CNO particles can be affected by heat-treatment [33,34] and electron beam irradiation [35,36] methods. Their unique spherical symmetry leads to self-compression [37]. The distance between the graphitic shells is smaller than the corresponding distance in graphite (0.335 nm) and can reach values as low as that present in diamond (diamond planes are separated by a distance of 0.206 nm) [38,39]. Transformation of spherical carbon nano-onions to diamond by low-temperature heat treatment at 500 °C in an air atmosphere was already observed by Tomita et al. [33,34]. X-ray diffraction studies using synchrotron radiation showed transformation of the diamond nanoparticles with an sp^3 hybridization into sp^2 carbons upon increasing the temperature [33]. After vacuum annealing of NDs, the resulting carbon nano-onion structures exhibit a mostly closed graphitic surface with little or no defects.

The physical and electrical properties of CNOs are a function of their synthesis temperature [17–19]. A constant capacitance over a large scan rate is one of the useful properties of carbon nano-onion electrodes [17,18] but additional studies of the electrochemical properties of CNOs prepared at different temperatures are still needed. It was already observed that the capacitive properties of the CNOs are a function of the annealing temperature used during their formation from NDs [40], the chemical nature of the CNO surfaces [41], and of their functionalization with other moieties [5–7]. Such structural modifications of CNOs have a significant effect on the orientations of the ions at the electrode–electrolyte interface and may have an influence on the electrical double-layer properties [2,9,10,17,18]. It has been shown experimentally and theoretically that size, geometry, and orientation of the ions have a very significant effect on the properties of the electrical double-layer [2,9,10,17,18]. However, not much is known about the inorganic electrolyte interactions with a post-modified CNOs under low-temperature annealing conditions.

Since knowledge of the structural properties of the carbon nano-onions is crucial to fully understand their physical and chemical properties for further applications, detailed studies are required. In order to further improve the conductivity of carbon nano-onions, further modifications of their surface via annealing resulted in graphitization of the carbon layers. Carbon nano-onions were formed by annealing of 5 nm nanodiamonds powder at 1650 °C in a low pressure He atmosphere [16]. Further low-temperature annealing, defined as a post-modification process, in an air atmosphere at 450 °C in the presence of carbohydrates: glucose (G) or starch (S), was performed to investigate the effect of the carbon microstructure on the specific capacitance and ion transport. It was already observed that the electrode conductivities are associated to defect densities [2] and micro- and mesoporous structures [42–44]. Therefore the electrical conductivity of carbon nano-onions increases with the annealing temperature due an increase of the graphitization [2].

The template technique based on the carbonization of organic precursors allows the preparation of three-dimensional carbon structures or the modification of existing nanostructured surfaces. Carbohydrates are natural carbon precursors with a 3D structure that contain networks of mainly sp^2 and sp^3 bonded atoms. Carbonization of carbohydrates is frequently reported as a cheap and easy way to prepare carbon spheres with a high number of functional groups [45]. The method, often described as a facile green-chemistry one, was used for the preparation of porous carbon materials from carbohydrates with a metal salt [46] and inorganic nanocolloids [47]. Another advantage of using these molecules in the annealing process is their low carbonization temperature, about 400 °C. Therefore, the carbonization of carbohydrates on the surface of CNOs allowed the preparation of three-dimensional porous structures, including micro- and

mesopores, and introduced chemical functionalities based mainly on oxygen-containing groups. Modification of CNO surfaces led to enhanced charge storage performance.

2. Experimental section

2.1. Chemicals

All chemicals and solvents used were commercially available and used without further purification: glucose (⩾ 99.5% (GC), Sigma–Aldrich), starch (puriss. p.a., from potato, reag. ISO, reag. Ph. Eur., soluble, Sigma–Aldrich) tetraoctylammonium bromide (⩾ 98%, Fluka), sodium chloride (~98%, Sigma–Aldrich), lithium perchlorate (98+%, Sigma–Aldrich), sodium perchlorate (98+%, Sigma–Aldrich), tetraethylammonium chloride hydrate (Sigma–Aldrich), and anhydrous ethanol (99.8%, Poch Gliwice), nanodiamond powder (Carbodeon uDiamond® Molto) with a crystal size between 4 and 6 nm, and nanodiamond content ⩾ 97 wt.%. All aqueous solutions for electrochemical studies were made using deionized water, which was further purified with a Milli-Q system (Millipore).

2.2. Apparatus and instrumentation

The films were imaged by secondary electron SEM with the use of an S-3000 N scanning electron microscope from FEI (Tokyo, Japan). The accelerating voltage of the electron beam was either 15 or 20 keV and the working distance was 10 mm. Transmission Electron Microscope images were recorded using the FEI Tecnai™ instrument. The accelerating voltage of the electron beam was 200 keV. Thermogravimetric experiments were performed using SDT 2960 Simultaneous TGA-DTG-DTA (TA Instruments company). The spectra were collected at 10 °C min^{-1} in an air atmosphere (100 mL min^{-1}).

Prior to gas sorption analysis, all samples were degassed at 300 °C at low vacuum (0.2 torr) for 24 h to remove any adsorbed species. N_2 gas sorption measurements were performed using a Micromeritics apparatus (ASAP2405-6-channel automatic sorption analyzer, Micromeritics Corp., USA) at −196 °C.

The room temperature Raman spectra in the range between 100 and 3500 cm^{-1} were investigated with a Renishaw Raman InVia Microscope equipped with a high sensitivity ultra–low noise CCD detector. The radiation from an argon ion laser (514 nm) at an incident power of 1.15 mW was used as the excitation source. Raman spectra were acquired with 3 accumulations of 10s each, 2400 l mm^{-1} grating and using a 20x objective.

Voltammetric experiments were performed using an AUTOLAB (Utrecht, The Netherlands) computerized electrochemistry system equipped with a PGSTAT 12 potentiostat using a three-electrode cell placed in a Faraday cage. The AUTOLAB system was controlled with the GPES 4.9 software of the same manufacturer. A glassy carbon disk electrode (Bioanalytical Systems Inc.) with a diameter of 3 mm (Bioanalytical Systems Inc.) was used as the working electrode. The surface of the electrode was polished using extra fine carborundum paper (Buehler) followed by 0.3 μm alumina and 0.25 μm diamond polishing compound (Metadi II, Buehler). The electrode was then sonicated in water in order to remove traces of alumina from the metal surface, washed with water, and dried. The counter electrode was a platinum flag with an area of about 0.5 cm^2. A silver wire immersed in 0.1 mol L^{-1} AgCl and separated from the working electrode by a ceramic tip (Bioanalytical Systems Inc.) served as the reference electrode. All experiments were done in water purified through a Millipore apparatus. Oxygen was removed from the solution by purging with argon.

2.3. Annealing of CNOs

The plain CNOs (synthesized at 1650 °C, defined as CNOs) were obtained by annealing nanodiamonds following by procedure already published [16,48]. Commercially available nanodiamond powder (Carbodeon uDiamond® Molto) with a crystal size between 4 and 6 nm, and nanodiamond content ⩾ 97 wt.%, were used for the preparation of CNOs. NDs were placed in a graphite crucible and transferred to an Astro carbonization furnace. The air in the furnace was removed by applying a vacuum followed by purging with helium. The process was repeated twice to ensure complete removal of air. Annealing of ultradispersed nanodiamonds was performed at 1650 °C under 1.1 Pa He atmosphere with a heating ramp of 20 °C min^{-1}. The final temperature was maintained for 1 h, then the material was slowly cooled to room temperature over a period of one hour. The furnace was opened, and the transformed CNOs were annealed in air at 400 °C to remove any amorphous carbon. Next, post-modification of CNOs with glucose (G) or starch (S) was performed at 450 °C in an air atmosphere, and these resulted in modified CNOs (m-CNOs): m-CNOs, m-CNOs/G, and m-CNOs/S. The black carbohydrate-derived CNO products, were prepared via annealing (1 h) of 10 mg of CNOs and 5 mg G or 5.1 mg S; annealing (2 h): (a) 10 mg of CNOs and 5 mg G or 5.1 mg S, (b) 10 mg of CNOs and 9.9 mg G or 9.8 mg S. The mixing of CNOs with carbohydrates was performed in the solid phase using mortar and pestle.

2.4. Preparation of CNO films

2 mg of CNOs, m-CNOs, m-CNOs/G or m-CNOs/S were dispersed with the aid of ultrasonic agitation in 500 μL ethanol to give a 4 mg mL^{-1} black suspension. The CNO films were prepared by the drop cast-method: 10 L of CNO (4 mg mL^{-1}) solution with 10 mmol L^{-1} TOABr.

3. Results and discussion

3.1. Structural characterization of plain and post-modified CNOs

Carbon nano-onions possess concentric-shells, with an intershell distance that depends on the annealing temperature during their production [15,25,28,33,34]. High-resolution transmission electron microscopy (HRTEM) enables detailed imaging of the CNO structures and the evolution of their curved graphitic layers as a function of annealing time and/or temperature. Transmission electron microscopy observations of CNOs showed spherical shapes ranging between 3 and 40 nm diameters (Fig. 1a) with 80% of 6–11 layered CNOs

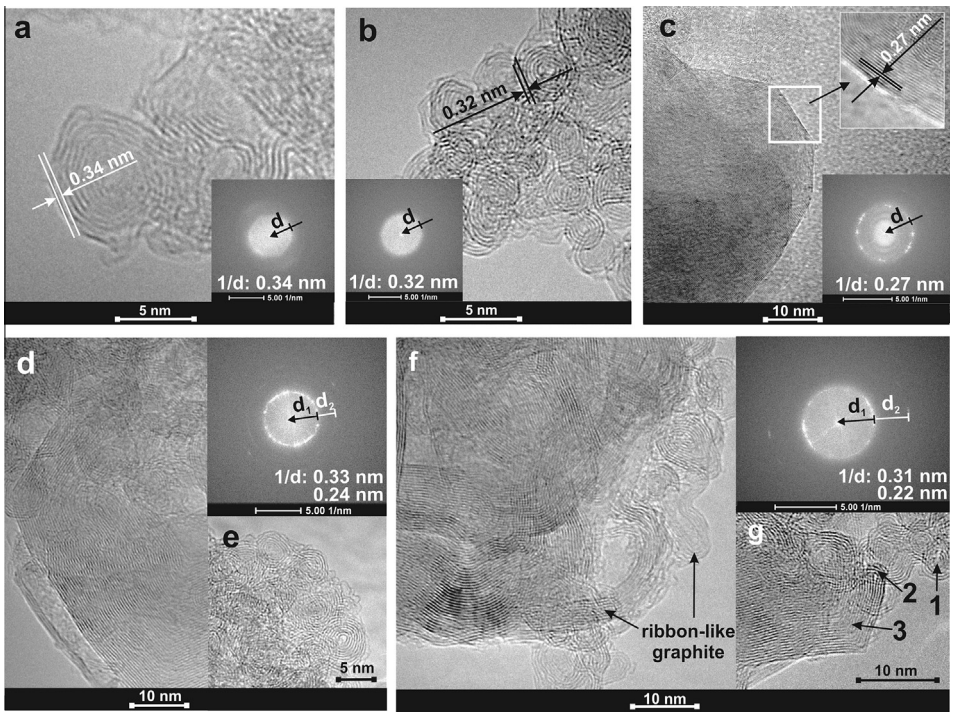

Fig. 1 – HRTEM images of (a) CNO; post-modified at 450 °C: (b, c) m-CNO (post-modified 1 h); (d, e) m-CNO/G (post-modified 1 h; m_{CNO}:m_G = 2:1), (f) m-CNO/S (post-modified 2 h; m_{CNO}:m_S = 1:1), and (g) m-CNO/S (post-modified 1 h; m_{CNO}:m_S = 2:1).

(5–9 nm). The central fullerene at the core of the CNOs is surrounded by multiple layers of nested concentric graphitic shells (with I_h symmetry) with an intershell spacing estimated from TEM diffraction patterns around 0.34 nm [33,34,45], similar to highly oriented pyrolitic graphite (HOPG) [49]. A post-modification process occurring under the low-temperature annealing process in air appears to lead to CNO compression, graphitization and polygonization (faceting structure) [28,32,34]. After post-modification, the onions are in a compressed state and the spacing between the CNO layers range from 0.33 nm to 0.27 nm (Fig. 1b, c). Such behavior was also observed while annealing nanodiamond particles at 1800 °C in an inert atmosphere [50].

Graphitization of the CNOs was observed to be more pronounced when post-modified in the presence of carbohydrates (Fig. 1e, g). TEM diffraction patterns indicate that the intershell interaction in CNO and m-CNO are much weaker when compared with those in m-CNO/G and m-CNO/S. The distances of the intershell spacing estimated from TEM diffraction patterns are between 0.32 nm (Fig. 1b) and 0.22 nm (Fig. 1f). Thus annealing results in CNO structures that are more diamond-like (diamond planes are separated by a distance of 0.206 nm) [39]. Therefore, the distances between the graphene interlayers and the structures of the spherical CNOs depend on the annealing conditions, such as time (1 h or 2 h) and the mass ratio of CNOs to carbohydrates (m_{CNO}:$m_{carbohydrates}$ = 1:1 or 2:1). Longer heating times (2 h) and higher mass ratios of carbohydrates to CNOs (m_{CNO}:$m_{carbohydrates}$ = 1:1) lead to the destruction of some spherical structures of the CNOs (Fig. 1f, g). A post-modification low-temperature annealing process of CNOs in the presence of carbohydrates led to the formation of non-homogeneous products. The thickness of the carbohydrate coating can be easily controlled by varying the carbohydrate mass during the post-modification low-temperature annealing process (Fig. 1f, g). The interior structure of some CNOs still exhibits the atomic layer planes (Fig. 1e and structure 1 in 1 g). Notably, in some onions the annealing process appears to disrupt the integrity of the graphene layers (Fig 1f, structure 2) or form ribbon-like graphite structures (Fig. 1f). The curved graphitic layers of CNOs in the presence of carbohydrates and an air atmosphere are metastable and tend to link and form graphitic ribbons, comparable to annealed NDs at low-temperatures [51]. Enoki et al. [52,53] and Kuznetzov et al. [54–56] have demonstrated that impurities (oxygen and hydrogen containing gasses) during the annealing process of NDs lead to carbon redistribution in nanocarbons with a low surface energy. Based on molecular dynamic simulations Ponomareva et al. [57] suggested the following mechanistic steps for CNO transformation into diamond-like structures: (i) under heating the most strained regions (pentagons) in the fullerene shells of the onion are destroyed and this results in the formation of holes and in a reduction of the interlayer spacing in the onion; (ii) during hole formation, the free atoms produced move to the outer shells, which can form new fullerene shells due to the additional reduction of the interlayer spacing; and (iii) reduction of the interlayer spacing acts as a 'microscopic pressure chamber', in which the diamond-like structures are formed.

A post-modification process of the CNOs was affected by a low-temperature annealing procedure in an air atmosphere without or in the presence of carbohydrates. This process altered their textural properties and is in agreement with the gas adsorption measurements. The adsorption and desorption

characteristics of nitrogen, the micro- and mesopore structure, the pore volume and the specific surface area of all types of CNOs were measured by multilayer model of coverage adsorption, the Brunauer–Emmett–Teller (BET) static nitrogen adsorption technique [58].

Based on Eq. (1), there should be a linear relationship between the specific capacitance (C) and the specific surface area (SSA). The BET specific surface areas (S_{BET}) were obtained from linear plots of $1/[Q(p/p_0) - 1]$ vs. the relative pressure (p/p_0), where Q is the weight of adsorbed gas (Fig. 2a). An S_{BET} of 412 $m^2\ g^{-1}$ was obtained for plain CNOs, very close to the value for ideal spherical solid particles. Structures with a diameter of 5 nm would correspond to an S_{BET} valve of 343 $m^2\ g^{-1}$ [15], based on the known density of diamond (3.5 g cm^{-3}) and for graphitic carbon (2.2 g cm^{-3}). The S_{BET} for diamond and graphitic carbon corresponds to 343 $m^2\ g^{-1}$ and 545 $m^2\ g^{-1}$, respectively [15]. The surface area of the CNOs increased after post-modification due to additional graphitization, and reached a maximum of 511 $m^2\ g^{-1}$ for m-CNOs/S (Table 1), which is consistent with the TEM measurements. However,

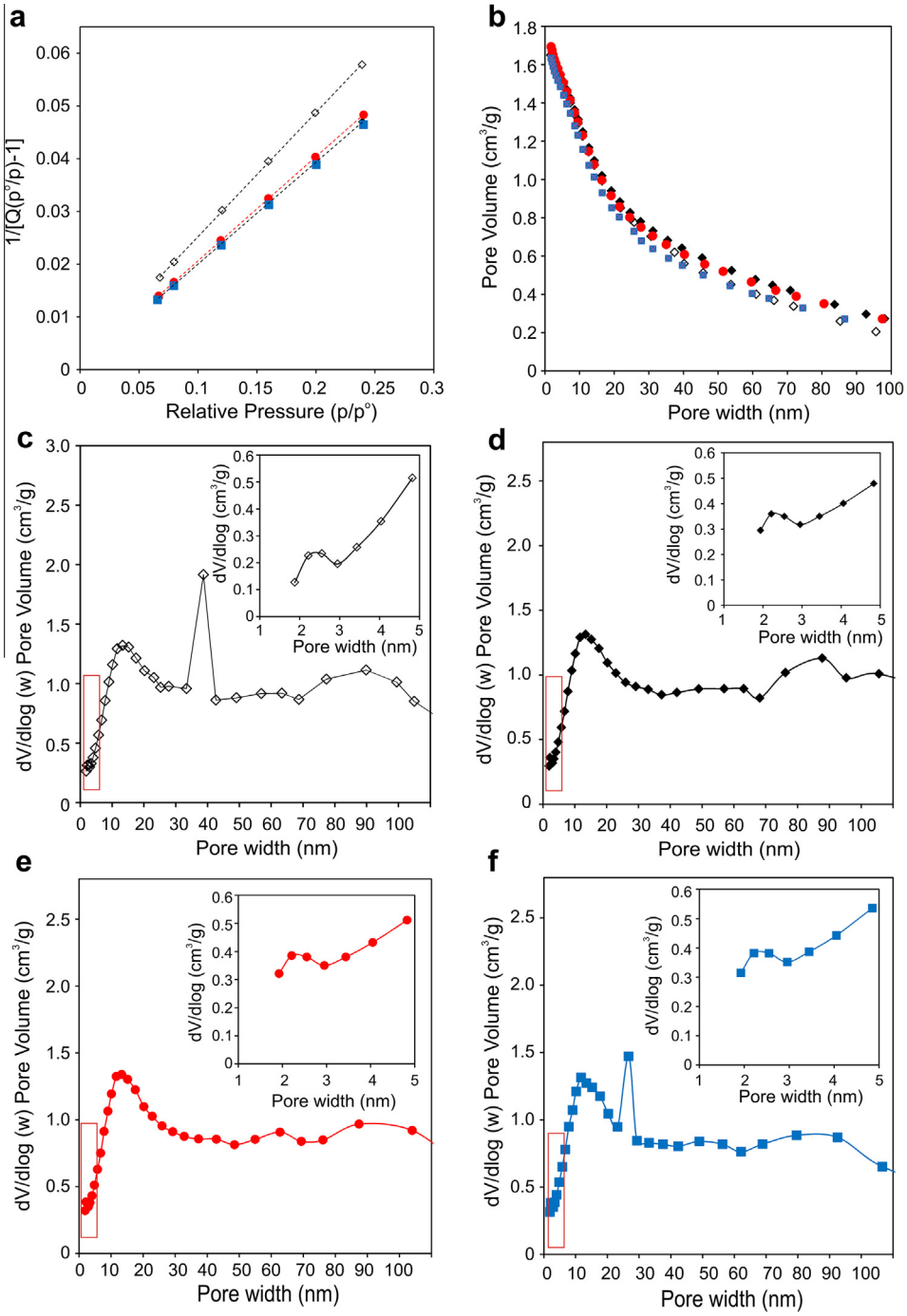

Fig. 2 – (a) BET surface area plot, (b) BJH Desorption Cumulative Pore Volume, and (c, d, e, f) BJH Desorption dV/dlog(w) Pore Volume for: (◊) CNO, (♦) m-CNO, (●) m-CNO/G, and (■) m-CNO/S composites. (A colour version of this figure can be viewed online.)

Table 1 – Textural parameters of plain and post-modified CNOs in the presence/absence of carbohydrates according to N_2 adsorption/desorption isotherms.

Sample	S_{BET}[c] ($m^2\ g^{-1}$)	Micropore area ($m^2\ g^{-1}$)[d,f]	Total pore volume of pores width[e] (V_T, $cm^3\ g^{-1}$ nm)	Pore volume (V_p, $cm^3\ g^{-1}$)	Pore size (nm)
Diamond	343[g]		–	–	–
Graphitic carbon	545[g]		–	–	–
CNOs	411.5	28.5	110.6	1.69	12.6
m-CNOs[a]	503.3	75.7	120.7	1.75	12.9
m-CNOs/G[a,b]	491.8	61.8	134.4	1.78	12.3
m-CNOs/S[a,b]	511.3	66.4	156.8	1.78	11.8

[a] Post-modification by low-temperature annealing (1 h) in an air atmosphere.
[b] Mass ratio CNOs:carbohydrates (2:1).
[c] S_{BET} – BET specific surface area.
[d] Based on t-Plot method.
[e] Single point desorption total pore volume of pores less at relative $p/p^\circ = 0.987$.
[f] Barret–Joyner–Halenda (BJH) desorption average pore width (4 V/A).
[g] From Ref. [15].

TEM studies clearly showed that the polygonization of CNOs during the post-modification process occurred and corresponded to the creation of some diamond-like structures, although the spherical-CNO, and ribbon-like graphitic structures are still predominant, as confirmed by the increasing S_{BET} values (Table 1).

Barret–Joyner–Halenda (BJH) proposed a calculation method for the distribution curves of the pore volume (dV_p/ dd_p) or of the surface area (dS/ dd_p) as a function of pore diameter (d_p) from nitrogen adsorption–desorption data [59]. Starting from the isotherm it's possible to correlate the necessary gas volume to fill all the pores in the materials, considering their cylindrical form, according to the formula:

$$d_p = \frac{4V_p}{S_{BET}} \quad (2)$$

where: d_p is the average pore diameter (nm); V_p is the pore volume ($cm^3\ g^{-1}$) and S_{BET} is the specific surface area ($m^2\ g^{-1}$). As the post-modification processes occurred, the pore volume, V_P, increased from 1.69 to 1.78 $cm^3\ g^{-1}$ for CNOs and m-CNO/G or m-CNO/S, respectively (Table 1).

Average pore sizes were also estimated from the pore volume, which is derived from the amount of N_2 vapor adsorbed at a relative pressure close to unity (t-Plot method and BJH model). It was observed that the average pore size of ~12 nm did change significantly with the post-modification treatment of CNOs in the presence or absence of carbohydrates. According to the pore size distribution curves of the BJH adsorption, it was also possible to estimate the pore size distribution of CNOs. Plain as well as post-modified CNOs have mainly mesoporous structures, with pores in the 2–50 nm diameter range. Moreover, as shown in Table 1, there is a small fraction of micropores (< 2 nm) available in all of the CNO materials. Post-modification of CNOs led to more micropores in the CNO samples, and the total surface area of the micropores increased from 7% to 15% (t-Plot method). Therefore, the wider range of the pore sizes at a relative pressure close to unity from 110.6 to 156.8 $cm^3\ g^{-1}$ nm were observed (Table 1), indicated that the structure of the pores changed more to the micro- and mesoporous domain.

Another method, differential-thermogravimetric analysis (TGA-DTG-DTA), was performed to probe the thermal stability of CNOs and m-CNOs. The temperature necessary for the removal of the porous carbon formed during the post-modification occurring in low-temperature annealing in an air atmosphere is lower than the decomposition temperature of the pristine carbon nanostructures. Fig. 3 shows TGA-DTG-DTA scans under an air atmosphere for the post-modified CNO/G and CNO/S (Fig. 3e, f), and the reference materials modified using the same experimental conditions (Fig. 3c, d, b, a, respectively). The degree of graphitization of the CNOs could be studied using TGA-DTG-DTA [60]. According to the results presented by Chen et al. [61] the higher the oxidation temperature the better graphitized carbon nanostructures are obtained. The onset oxidation and end temperatures are listed in Table 2, representing the initial weight loss, the maximum weight loss, and the final weight in the TGA-DTG-DTA graphs, respectively. A higher inflection temperature was observed for the o-CNOs (I_t = 617 °C) than for those annealed at 450 °C in an air atmosphere (I_t = 575 °C), and the temperature range between onset and end temperatures is wider, indicating a polycrystalline character of the resulting CNO structures. There is no weight loss or very small loss at temperatures between 200 and 400 °C, showing the small content of amorphous carbon in the plain CNO samples (Fig. 3a).

Introducing carbohydrates during CNO annealing is expected to change the thermal properties of the carbon nanoparticles. Fig. 3 shows the TGA-DTG-DTA thermograms of annealed carbohydrates: G and S alone, that lose ca. 10% of their original weight under an air atmosphere at 200 °C (Fig. 3c, d, respectively). Exothermic peaks in the calorimetric curves between 50 and 130 °C often correspond to the crystallization process of the amorphous carbohydrates [61]. On continued heating, further thermal decomposition of the carbohydrate materials is observed at ca. 600 °C. Carbohydrates G and S were decomposed at 515.8 and 471.5 °C, respectively. For m-CNOs, a 96% weight loss is observed for both samples: m-CNO/G and m-CNO/S (Figs. 3e, f). However, the TGA-DTG-DTA plots for m-CNO/G and m-CNO/S samples (Figs. 3e, f) did not give evidence for the detachment of annealed-carbohydrates from the surface of the carbon

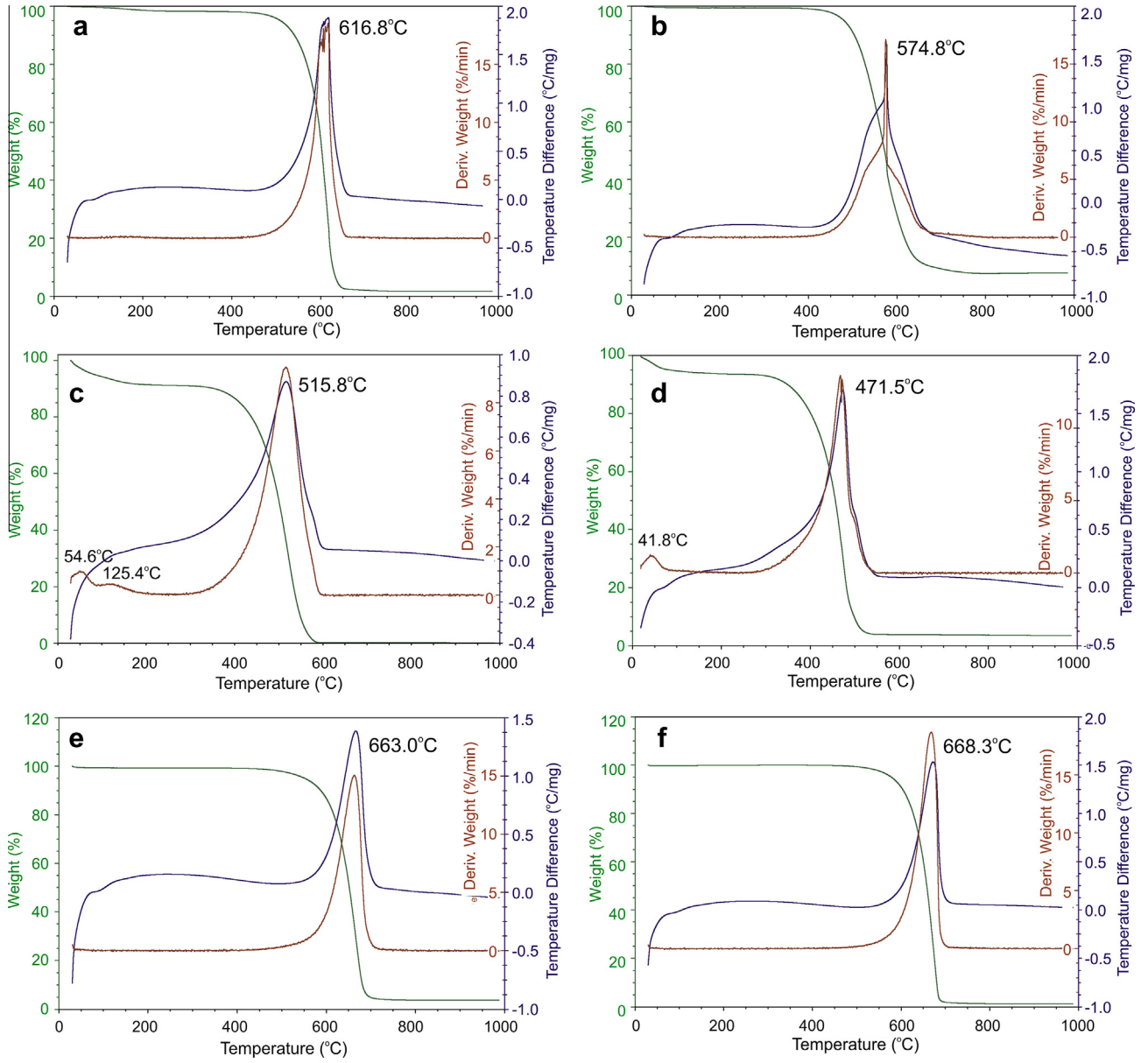

Fig. 3 – TGA-DTG-DTA curves for (a) CNO, (b) m-CNO, (c) G annealed at 450 °C, (d) S annealed at 450 °C, (e) m-CNO/G, and (f) m-CNO/S composites in an air atmosphere at 10 °C min^{-1}. Annealing (1 h) of CNOs was performed in an air atmosphere, mass ratio m_{CNOs}:$m_{carbohydrates}$ = 2:1. (A colour version of this figure can be viewed online.)

Table 2 – The TGA-DTG-DTA results of plain and post-modified CNOs in the presence/absence of carbohydrates.

Sample	Onset temperature (°C)	Inflection temperature (°C)	End temperature (°C)	Weight loss (%)
CNOs	520	616.8	650	97
m-CNOs[a]	470	574.8	750	92
G[a]	310	515.8	620	96
S[a]	280	471.5	570	96
m-CNOs/G[a,b]	420	663.0	740	96
m-CNOs/S[a,b]	470	668.3	730	99

[a] Post-modification by low-temperature annealing (1 h) in an air atmosphere.
[b] Mass ratio CNOs:carbohydrates (2:1).

nanostructures during continued annealing. The observed shifts of the inflection temperature up to 660 °C confirm that there are structural changes of the CNOs during their annealing in the presence of carbohydrates. All observed processes

have exothermic character (Fig. 3a–f), corresponding to decomposition of the materials.

Raman spectroscopy is very informative for the characterization of the chemical structure of a variety of polymorphic carbon samples. The most intense *G* (Graphite) and *D* (Disorder) bands can be used to characterize the crystal size and they can provide quantitative information about sample composition and about the degree of disorder and the sp^2–sp^3 ratio of carbon atoms in the sample [62]. The *G* band is related to the C—C vibration of the carbon materials with sp^2 orbital structures and the *D* band arises from the disorder-induced vibration of the C—C bond. Raman spectroscopy is frequently used to characterize the "quality" of the CNOs, that is, the presence of imperfections in the graphene planes of the carbon nano-onions [63,64].

The post-modification low-temperature annealing process resulted in the transformation of spherical carbon nano-onions into different onion-like structures with different sizes and shapes. Such transformations result in non-homogeneous materials with different Raman characteristics (Fig. 1). The Raman spectra presented in Fig. 4a, b, corresponding to CNOs and m-CNOs (2 h), respectively, showed graphitic or diamond-like structures. For single crystals of highly oriented pyrolitic graphite (HOPG), the line at 1582 (±5) cm^{-1} (*G* line) is assigned to the E_{2g} species of the infinite crystal [65,66]. For samples with small crystal planar domain sizes L_a, a doublet structure at about 1580 cm^{-1} is observed [67]. The higher-frequency component of this doublet is observed at about 1620 cm^{-1} (*D'*band) and is often observed in highly-defective graphite [68]. In the Raman spectrum of small graphite crystallites, the *D* line appears at about 1355 cm^{-1} [46]. The band is attributed to the A_{1g} mode of the small crystallites or boundaries of larger crystallites of graphite. For diamond a single *D* line is observed at 1332 cm^{-1} and it is related to the zone-center optical phonon with F_{2g} symmetry [69]. The *2D* band originates from a two phonon double resonance Raman process. The broad *2D* band is an indication of multilayer graphene and its electronic band structure [70].

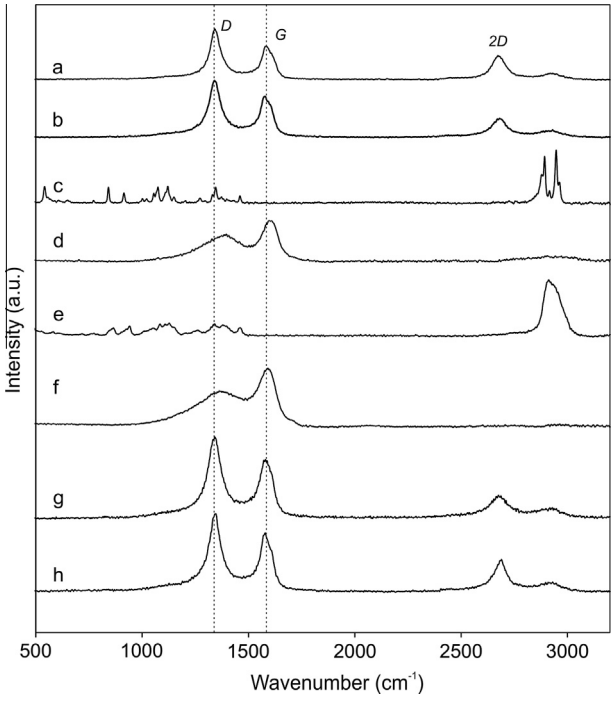

Fig. 4 – Raman spectra of (a) CNOs, (b) m-CNOs, (c) non-annealed G, (d) m-G, (e) non-annealed S, (f) m-S, (g) m-CNO/G, and (h) m-CNO/S recorded at λ_{exc}=514 nm. Post-modification of CNOs was performed in an air atmosphere (1 h), mass ratio m_{CNOs}:$m_{carbohydrates}$ = 2:1.

Raman spectra of plain and post-modified CNOs in the presence/absence of carbohydrates are shown in Fig. 4 and the corresponding data are collected in Table 3. The *D* and *G* lines are intense and broad, which indicates the mixed-phases of carbon nano-onion materials [51]. Furthermore, the *D* band is stronger than the *G* band for CNOs, m-CNO/G, and m-CNO/S. The *D*-band in graphite involves scattering from a defect which breaks the basic symmetry of the graphene sheet with sp^2 carbons containing pores, impurities or other symmetry-breaking defects. In this respect our spectra are similar to those of strongly disordered graphene [71].

The decrease of the intensity ratio of I_D/I_G is an indication of an increase of the number of additional sp^2 carbons in the graphitic layers [73]. After annealing of plain G and S at 450 °C, broad bands at about 1377 cm^{-1}, and at 1582 cm^{-1} were observed (Fig. 4d, f). The results suggest that after annealing the carbohydrates, the resulting networks contain mainly sp^2 and sp^3 bonded atoms. The I_D/I_G ratio is 1.71 for plain CNOs and ~1.4 for m-CNO/carbohydrates (Fig. 4b, g, h, Table 3), suggesting the successful modification of the CNO surface.

3.2. *Morphology characterization and electrochemical studies of CNO films*

Electrochemical applications of carbon materials depend on their wettability and intrinsic conductivities and the specific capacitances (F g^{-1}) depend on the degree of particle agglomeration in the film, particle size, and other structural properties, and defects on the surface of the nanostructures [2,8–10]. It was already observed that chemical heterogeneities, surface functionalities, and micro-mesoporous structures significantly influence the electrochemical behavior of porous carbon electrodes and contribute to the increase in the total capacitance of electrical double layer capacitors [8–10]. Post-modification of CNOs in an air atmosphere in the presence/absence of carbohydrates changed their specific surface area and pore size distributions. High surface areas and microporosities are required for high performance supercapacitors [2,8–10].

Morphological characterization is a direct way to evaluate the degree of the dispersion state of materials. SEM images of a Au foil covered with plain and post-modified CNOs in the presence/absence of carbohydrates are shown in Fig. 5. The CNO films exhibit porous morphologies, with many channels and outcroppings (Figs. 5a, b, e, f). However, post-modification by low-temperature annealing did not change significantly the initial morphological properties of the carbon materials (inserts in Fig. 5a, b), but further temperature-modification of the CNOs in the presence of carbohydrates did alter their surfaces (Fig. 5e, f). Therefore, annealing of CNOs in the presence of the carbohydrates gave rise to increased solubility and

Table 3 – Best fit frequencies for the *D* and *G* bands obtained at 514 nm laser excitation energies, and relative intensity I_D/I_G.

Sample	*D*	*G*	I_D/I_G
CNOs	1331	1568	1.71
m-CNOs[a]	1335	1560	1.37
m-CNOs/G[a,b]	1332	1570	1.41
m-CNOs/S[a,b]	1330	1570	1.40

[a] Post-modification by low-temperature annealing (1 h) in an air atmosphere at 450 °C.
[b] Mass ratio CNOs:carbohydrates (2:1); the peak fitting was done using a formula obtained after computer deconvolution [72].

ease of surface film formation (Fig. 5e, f). The morphology of the annealed carbohydrates (Fig. 5c, d) differs from those of films formed from non-annealed ones (inserts in Fig. 5c, d). These morphological variations have a influence on the capacitive behavior of the CNOs.

For the electrochemical studies, plain CNOs and m-CNOs were immobilized in thin films of tetra(*n*-octyl)ammonium bromide (TOABr). TOABr ensures good mechanical and electrochemical stability of the CNO films without causing changes in the capacitve currents. This procedure has been frequently used to study the electrochemical behavior of fullerenes and carbon nanostructures in aqueous solutions [74–76]. A drop of ethanol containing CNOs and 10 mmol L^{-1} TOABr were deposited on the electrode surface. The electrodes modified with the CNO films were then transferred to an aqueous solution containing 0.1 mol L^{-1} supporting electrolyte. The films exhibit good mechanical and electrochemical stability under cyclic voltammetric conditions. The voltammetric responses of layers including the plain and post-modified CNOs are shown in Fig. 6.

Fig. 6 shows a comparison of the electrochemical properties of the plain (Fig. 6 curve 1) and post-modified CNOs (Fig. 6 curves from 2 to 6) in TOABr films. In every case, the amount of CNOs in the film was the same. The films exhibit

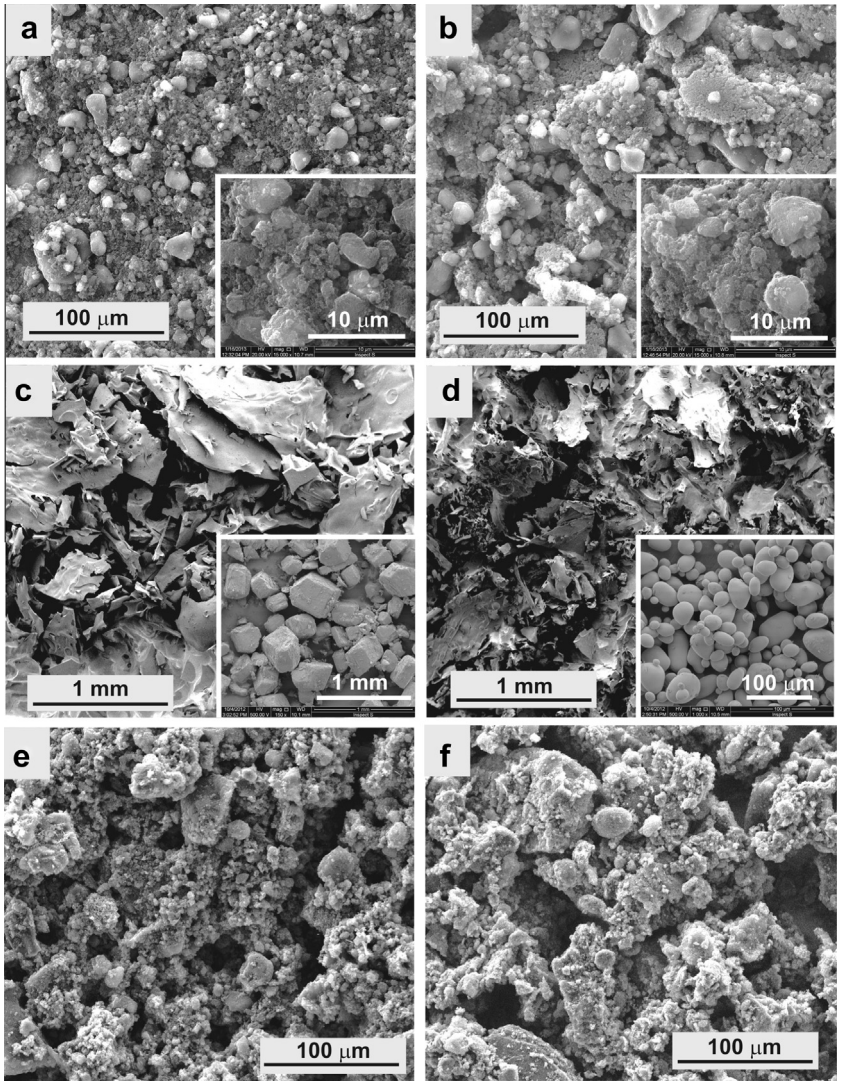

Fig. 5 – SEM images of the Au foil covered with (a) CNO, (b) m-CNO, (c) m-G, insert: G before annealing, (d) m-S, insert: S before annealing, (e) m-CNO/G, and (f) m-CNO/S composites. Post-modification (1 h) at 450 °C, m_{CNOs}:$m_{carbohydrates}$ = 2:1. Films prepared in ethanol solution with 10 mmol L^{-1} TOABr.

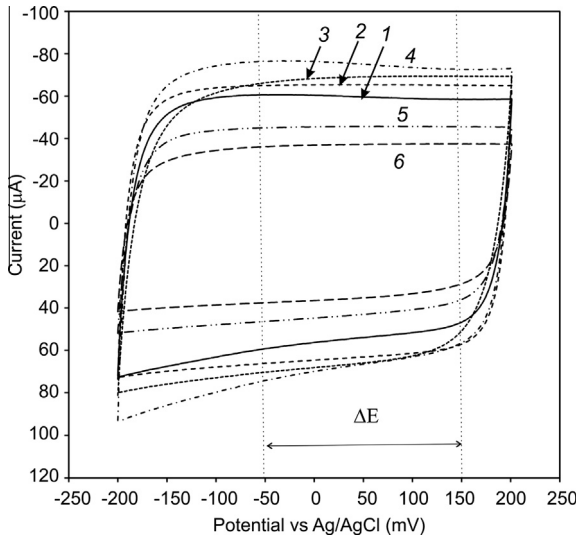

Fig. 6 – Cyclic voltammograms of a GC electrode covered with 10 mmol L^{-1} TOABr and (1) CNO; (2) m-CNO; (3) m-CNO/G (1 h, m_{CNOs}:$m_{carbohydrates}$ = 2:1); (4) m-CNO/S (1 h, m_{CNOs}:$m_{carbohydrates}$ = 2:1); (5) m-CNO/S (2 h, m_{CNOs}:$m_{S=}$2:1), and (6) m-CNO/S (2 h, m_{CNOs}:$m_{S=}$1:1). Sweep rate 20 mV s^{-1} in 0.1 mol L^{-1} NaCl.

typical capacitive behavior with almost pseudo-rectangular cathodic and anodic profiles, characteristic of ideal capacitors. Moreover, multi-scan CVs show that the films are stable, after 300 complete CV cycles, approximately 91% of the initial capacitance was preserved. The potential can be cycled between +0.20 and –0.20 V (vs. Ag/AgCl) without any noticeable change in the shape of the voltammogram. Post-modification by low-temperature led to graphitization of the carbon structures, which has been shown to be beneficial for fast charge storing of m-CNOs/TOABr films (Fig. 6, curve 2). Therefore, the high degree of reversibility for double layers near the CNO film surface, indicates that there are no chemical processes or other changes occurring between charge and discharge cycles. The electrochemical properties of the m-CNO/G/TOABr or m-CNO/S/TOABr films depend also on the post-modification low-temperature annealing time of the carbon particles and the carbohydrate mass in the CNO composite. The longer the annealing time (2 h) and the higher the mass of the carbohydrates (m_{CNOs}:$m_{carbohydrates}$ = 1:1) present led to reduction of the specific capacitances.

The specific capacitance, C_s, was calculated based on the mass of the CNOs on the electrode surface, m, within the potential range, ΔE, (Fig. 6) according to the following equation:

$$C_s = \frac{\int i_c dt}{\Delta E m} \quad (3)$$

The capacitive current, i_c, depends sligthly on the CNO structures (Fig. 6, curves from 1 to 4). The specific capacitances of the CNO/TOABr films obtained by using plain or post-modified carbon nanostructures are collected in Table 4.

A linear dependence of the capacitance current with the sweep rate was observed up to 200 mV/s, as shown in Fig. 7a, c. Thus, the capacitive current, i_c, can be expressed by the following equation [8]:

$$i_c = C_s \upsilon m \quad (4)$$

where C_s is the specific capacitance, m is the mass of material deposited on the electrode surface, and υ is the potential sweep rate. Specific capacitances calculated from the slope of the i_c–υ linear relations (Fig. 7e) were equal to 14 F g^{-1} for both m-CNO/G and m-CNO/S composites.

Electrolyte wettability and orientation can be improved by structural modification of the carbon nanostructure's surface [77]. Therefore, the effect of the supporting electrolyte on the electrochemical properties of the plain and post-modified CNOs was investigated. Fig. 8 shows the voltammetric behavior of the CNO/TOABr films in the different supporting electrolytes at a sweep rate of 20 mV s^{-1}. The values of the specific capacitances, C_s, for the different inorganic supporting electrolytes are collected in Table 4. In all cases, specific capacitances in the presence of the inorganic electrolytes are affected by their nature.

The effects of the supporting electrolyte on the capacitances result from: (i) the degree of counter ion penetration, and (ii) the structure of the double layer on the CNO surface [78]. The electrochemical studies of the CNO/TOABr films

Table 4 – Specific capacitance of CNO films in aqueous solutions of different supporting electrolytes.

Supporting electrolyte	Specific capacitance (F g^{-1})[a,b]			
	CNOs	m-CNO[c]	m-CNO/G[c,d]	m-CNO/S
NaCl	11.09	12.14	12.77	13.93[c,d]
			13.81[g]	14.34[g]
	–	–	–	8.47[e,d]
	–	–	–	6.90[e,f]
$NaClO_4$	8.25	8.28	11.09	11.55[c,d]
$LiClO_4$	8.37	7.77	14.13	12.73[c,d]
$(Et)_4NCl$	6.47	5.26	8.88	9.51[c,d]

[a] At v = 20 mV s^{-1}.
[b] Integration ΔE (between 50 and −150 mV).
[c] Post-modification low-temperature annealing, 1 h at 450 °C.
[d] Mass ratio m_{CNO}:$m_{carbohydrates}$ = 2:1.
[e] Post-modification low-temperature annealing 2 h.
[f] Mass ratio m_{CNOs}:$m_{carbohydrates}$ = 1:1.
[g] From Ref. [15].

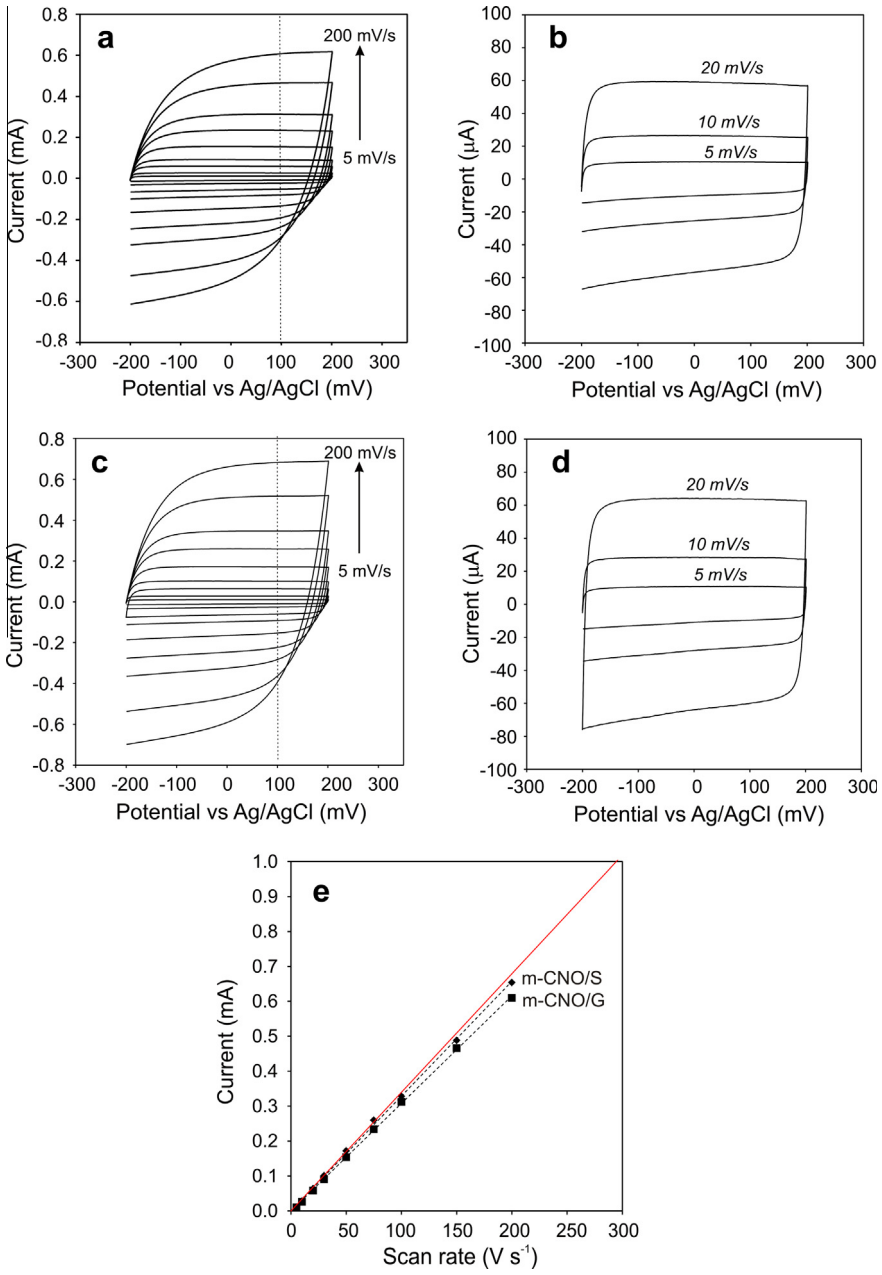

Fig. 7 – Cyclic voltammograms of a GC electrode covered with 10 mmol L^{-1} TOABr and (a, b) m-CNO/G and (c, d) m-CNO/S in 0.1 mol L^{-1} NaCl. The sweep rate was: 5, 10, 20, 30, 50, 75, 100, 150, and 200 mV s^{-1}. Post-modification occurred at 450 °C, 2 h; with mass ratio of m_{CNOs}:$m_{carbohydrates}$ = 2:1. (e) Dependence of the capacitive current with the sweep rate for m-CNOs/G and m-CNOs/S at 100 mV vs. Ag/AgCl. (A colour version of this figure can be viewed online.)

showed two trends: (i) CNOs and m-CNO films exhibit a more hydrophobic character with similar anion and cation influence on the capacitance; and (ii) the m-CNO/G and m-CNO/S films showed better accessibility and easier penetration of the inorganic counter ions. Hence, these results indicate that an adequate pore size is very important to obtain high values of the capacitance. Our studies showed that during the post-modification low-temperature annealing, textural characteristics of the CNOs changed, with an increase of the BET surface areas. These textural changes affected the electrochemical properties of post-modified CNOs and assured easy penetration of the supporting electrolyte in the m-CNO films. Further studies of CNO structural changes as a function of time, temperature, and atmosphere are required to fully understand the correlation between the physico-chemical properties of CNO particles with their electrochemical properties.

4. Conclusions

The post-modified CNOs using low-temperature annealing at 450 °C in an air atmosphere revealed different structures with spherical, polygonal concentric shells of CNOs, and ribbon-like graphitic structures. TEM, SEM, and TGA studies

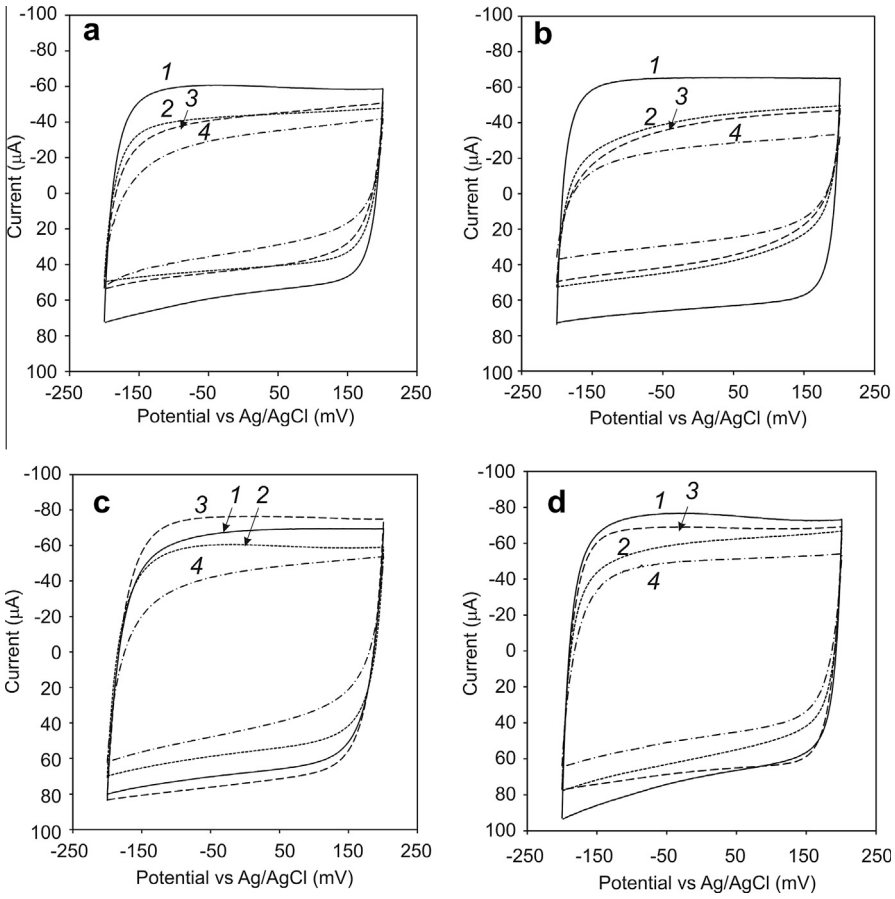

Fig. 8 – Cyclic voltammograms of GC electrode covered with 10 mmol L^{-1} TOABr, and (a) CNO, (b) m-CNO, (c) m-CNO/G, and (d) m-CNO/S in 0.1 mol L^{-1} different electrolyte (1) NaCl, (2) $NaClO_4$, (3) $LiClO_4$, and (4) $(Et)_4NCl$. The sweep rate was 20 mV s^{-1}.

showed graphitization of the CNOs, and their transformation upon annealing as a function of the ratio of the carbohydrate mass in the samples. Post-modification of CNOs by low-temperature annealing led to an increase of the BET specific surface area, with a maximum of 511 m^2 g^{-1} observed for m-CNOs/S. According to the pore size distribution curves of the BJH adsorption, the pore diameters were in the 2–50 nm range. Moreover, there is a small fraction of micropores (< 2 nm) available in all of the CNO materials. The electrochemical studies of the CNO/TOABr films showed two trends: (i) CNO and m-CNO films revealed more hydrophobic character with similar influence from anions and cations on the capacitance; and (ii) the m-CNO/G and m-CNO/S layers showed higher accessibility and easier penetration of the inorganic counter ions. Our studies provide the basis for further electrochemical applications of micro- and mesopores CNO structures.

Acknowledgments

We gratefully acknowledge Dr. Horst Reichert for pore and BET analysis from Micromeritics Analytical Services Europe and Dr. Robert Rybak for participation in discussions, from Syl&Ant Instruments. We gratefully acknowledge the financial support of the NCN, Poland, grant #2011/01/B/ST5/06051 to M.E.P.-B. L.E. thanks the Robert A. Welch Foundation for an endowed chair, grant #AH-0033 and the US NSF, grants: CHE-1110967 and CHE-1124075. SEM, TEM and Raman were funded by European Funds for Regional Development and National Funds of Ministry of Science and Higher Education, as part of the Operational Programme Development of Eastern Poland 2007-2013, project: POPW.01.03.00-20-034/09-00.

REFERENCES

[1] Geim AK, Novoselov KS. The rise of graphene. Nat Mater 2007;6:183–91.
[2] Portret C, Yushin G, Gogotsi Y. Electrochemical performance of carbon onions, nanodiamonds, carbon black and multiwalled nanotubes in electrical double layer capacitors. Carbon 2007;45(13):2511–8.
[3] Chen D, Tang LH, Li JH. Graphene-based materials in electrochemistry. Chem Soc Rev 2010;39(8):3157–80.
[4] Kovalenko I, Bucknall DG, Yushin G. Detonation nanodiamonds and onion-like-carbon-embedded polyaniline for supercapacitors. Adv Funct Mater 2010;20(22):3979–86.
[5] Plonska-Brzezinska ME, Breczko J, Palys B, Echegoyen L. Supercapacitors based on carbon nanostructure/polyaniline composites. ChemPhysChem 2013;14(1):116–24.

[6] Plonska-Brzezinska ME, Mazurczyk J, Breczko J, Palys B, Lapinski A, Echegoyen L. Preparation and characterization of first composites containing *small* carbon nano-onions and polyaniline. Chem Eur J 2012;18(9):2600–8.
[7] Plonska-Brzezinska ME, Lewandowski M, Błaszyk M, Molina-Ontoria A, Luciński L, Echegoyen L. Synthesis and properties of carbon nano-onion/PEDOT:PSS composites. ChemPhysChem 2012;13(18):4134–41.
[8] Conway BE. Electrochemical supercapacitors: scientific fundamentals and technological applications. Dordrecht, The Netherlands: Kluwer; 1999.
[9] Simon P, Gogotsi Y. Charge storage mechanism in nanoporous carbons and its consequence for electrical double layer capacitors. Phil Trans R Soc A 2010;368:3457–67.
[10] Lin R, Huang P, Segalini J, Largeot C, Taberna PL, Chmiola J. Solvent effect of the ion adsorption friom ionic liquid electrolyte into sub-nanometer carbon pores. Electrochim Acta 2009;54:7025–32.
[11] Ugarte D. Curling and closure of graphitic networks under electron-beam irradiation. Nature 1992;359:707–9.
[12] Iijima S. Direct observation of the tetrahedral bonding in graphitized carbon black by high resolution electron microscopy. J Cryst Growth 1980;50(3):675–83.
[13] Al-Jishi R, Dresselhaus G. Lattice-dynamical model for graphite. Phys Rev B 1982;26(8):4514–22.
[14] Suehiro J, Imasaka K, Ohshiro Y, Zhou G, Hara M, Sano N. Production of carbon nanoparticles using pulsed arc discharge triggered by dielectric breakdown in water. Jpn J Appl Phys 2003;42:L 1483–5.
[15] Roddatis VV, Kuznetsov VL, Butenko Y, Sua DS, Schlogla R. Transformation of diamond nanoparticles into carbon onions under electron irradiation. Phys Chem Chem Phys 2002;4:1964–7.
[16] Kuznetsov V, Chuvilin A, Butenko Y, Malkov I, Titov V. Onion-like carbon from ultra-disperse diamond. Chem Phys Lett 1994;222:343–8.
[17] McDonough JK, Frolov AI, Presser V, Niu J, Miller ChH, Ubieto T, et al. Influence of the structure of carbon onions on their electrochemical performance in supercapacitor electrodes. Carbon 2012;50(9):3298–309.
[18] Pech D, Burnett M, Durou H, Huang P, Mochalin V, Gogotsi Y, et al. Ultrahigh-power micrometer-sized supercapacitors based on onion-like carbon. Nat Nanotechnol 2010;5(9):651–4.
[19] Portret C, Chmiola J, Gogotsi Y, Park S, Lian K. Electrochemical characterization of carbon nanomaterials by the cavity microelectrode technique. Electrochim Acta 2008;53(26):7675–80.
[20] Gao Y, Zhou YS, Qian M, He XN, Redepenning J, Goodman P, et al. Chemical activation of carbon nano-onions for high-rate supercapacitor electrodes. Carbon 2013;51:52–8.
[21] Gu W, Peters N, Yushin G. Functionalized carbon onions, detonation nanodiamonds and mesoporous carbon as cathodes in Li-ion electrochemical energy storage devices. Carbon 2013;53:292–301.
[22] Koudoumas E, Kokkinaki O, Konstantaki M, Couris S, Korovins S, Detkov P, et al. Onion-like carbon and diamond nanoparticles for opical limitting. Chem Phys Lett 2002;357:336–40.
[23] Kuznetsov VL, Zilberberg IL, Butneko YV, Chuvilin AL, Segall B. Theoretical study of the formation of closed curved graphite-like structures during annealing of diamond surface. J Appl Phys 1999;86(2):863–70.
[24] Wang MS, Golberg D, Bando Y. Carbon "onions" as point electron sources. ACS Nano 2010;4(8):4396–402.
[25] Tomita S, Sakurai T, Ohta H, Fujii M, Hayashi S. Structure and electronic properties of carbon onions. J Chem Phys 2011;114(17):7477–82.
[26] Baowan D, Thamwattana N, Hill JM. Continuum modeling of spherical and spheroidal carbon onion. Eur Phys J D 2007;44:117–23.
[27] Ponomareva IV, Chernozatonskii LA. How can carbon onion transform into diamond-like structure. Microelectron Eng 2003;69:625–8.
[28] Xu Q, Zhao X. Bucky-diamond versus onion-like carbon: end of graphitization. Phys Rev B 2012;86:155417(1)–7).
[29] Mochalin VN, Shenderova O, Ho D, Gogotsi Y. The properties and application of nanodiamonds. Nat Nanotechnol 2011;7(1):11–23.
[30] Barnard AS. Theory and modeling of nanocarbon phase stability. Diamond Relat Mater 2006;15(2–3):285–91.
[31] Raty JY, Galli G, Bostedt C, Buuren TW, Terminello LJ. Quantum confinement and fullerene like surface reconstructions in nanodiamonds. Phys Rev Lett 2003;90(3):037401–4.
[32] Petit T, Arnault JC, Girard HA, Sennour M, Bergonzo P. Early stages of surface graphitization on nanodiamonds probed by X-ray photoelectron spectroscopy. Phys Rev B 2011;84(23):233407–12.
[33] Tomita S, Burian A, Dore JC, Lebolloch D, Fujii M. Diamond nanoparticles to carbon onions transformation: X-ray diffraction studies. Carbon 2002;40:1469–74.
[34] Tomita S, Fujii M, Hayashi S, Yamamoto K. Transformation of carbon onions to diamond by low-temperature heat treatment in air. Diamond Relat Mater 2000;9:856–60.
[35] Banhart F, Ayan PM. Carbon onions as nanoscopic pressure cells for diamond formation. Nature 1996;382:433–5.
[36] Redlich PH, Banhart F, Lyutovich Y, Ajayan PM. EELS study of the irradiation-induced compression of carbon onions and their transformation to diamond. Carbon 1998;36(5–6):561–3.
[37] Gan Y, Banhart F. The mobility of carbon atoms in graphitic nanoparticles studied by the relaxation of strain in carbon onions. Adv Mater 2008;20(24):4751–4.
[38] Huang JY. In situ observation of quasimelting of diamond and reversible graphite-diamond phase transformations. Nano Lett 2007;7(8):2335–40.
[39] Kuznetsov VL, Aleksandrov MN, Zagoruiko IV, Chuvilin AL, Moroz EM, Kolomiichuk VN, et al. Study of ultradispersed diamond powders obtained using explosion energy. Carbon 1991;29(4–5):665–8.
[40] Bushueva EG, Galkin PS, Okotrub AV, Bulusheva LG, Gavrilov NN, Kuznetsov VL, et al. Double layer supercapacitor properties of onion-like carbon materials. Phys Stat Sol (b) 2008;245(10):2296–9.
[41] Plonska-Brzezinska ME, Lapinski A, Wilczewska AZ, Dubis AT, Villalta-Cerdas A, Winkler K, et al. Solution ozonolysis of carbon nano-onions: synthesis, characterization and properties. Carbon 2011;49:5079–89.
[42] Frackowiak E, Beguin F. Carbon materials for the electrochemical storage of energy in capacitors. Carbon 2001;39:937–50.
[43] Raymundo-Pinero E, Kierzek K, Machnikowski J, Beguin F. Relationship between the nanoporous texture of activated carbons and their capacitance properties in different electrolytes. Carbon 2006;44:2498–507.
[44] Simon P, Gogotsi Y. Materials for electrochemical capacitors. Nat Mater 2008;7:845–54.
[45] Wen Z, Li J. Carbon nanocomposites as electrode materials for electrochemical energy storage, conversion and biosensor systems. J Mater Chem 2009;19:8707–13.
[46] Huang Y, Hu S, Zou S, Xu Z, Han Ch, Shen J. Mesoporous carbon materials prepared from carbohydrates with a metal chloride template. J Mater Chem 2009;19(41):7759–64.
[47] Lou XW, Chen JS, Chen P, Archer LA. One-pot synthesis of carbon-coated SnO_2 nanocolloids with improved reversible lithium storage properties. Chem Mater 2009;21(13):2868–74.

[48] Palkar A, Melin F, Cardona CM, Elliott B, Naskar AK, Edie DD, et al. Reactivity differences between carbon nano onions (CNOs) prepared by different methods. Chem Asian J 2007;2:625–33.
[49] Kroto HW. Carbon onions introduce new flavour to fullerene studies. Nature 1992;359:670–1.
[50] Akatyeva E, Huang JY, Dumitrica T. Edge-mediated dislocation processes in multishell carbon nano-onions. Phys Rev Lett 2010;105:106102(1)–4).
[51] Qiao Z, Li J, Zhao N, Shi Ch, Nash P. Structural evolution and Raman study of nanocarbons from diamond nanoparticles. Chem Phys Lett 2006;429:479–82.
[52] Prasad BLV, Sato H, Enoki T, Hishiyama Y, Kaburagi Y, Rao AM, et al. Heat-treatment effect on the nano-sized graphite p-electron network during diamond to graphite conversion. Phys Rev B 2000;62:11209–18.
[53] Enoki T. Diamond-to-graphite conversion in nanodiamond and the electronic properties of nanodiamond-derived carbon system. Phys Solid State 2004;46:651–6.
[54] Kuznetzov VL, Butenko YV, Zaikovskii VI, Chuvilin AL. Carbon redistribution processes in nanocarbons. Carbon 2004;42:1057–63.
[55] Obraztsova ED, Fujii M, Huyashi S, Kuznetzov VL, Butenko YV, Chuvilin AL. Closed curved graphite-like structures formation on micron-size diamond. Carbon 1998;36:361–7.
[56] Butenko YU, Kuznetzov VL, Chuvilin AL, Kolomiichuk VN, Stankus SV, Khairulin RA, et al. Kinetics of graphitization of dispersed diamonds in “low” temperatures. J Appl Phys 2000;88:4380–9.
[57] Ponomareva IV, Chernozatonskii LA. Coherent coexistence of nanodiamonds and carbon onions in icosahedral core–shell particles. Microelectron Eng 2003;69:625–8.
[58] Brunauer S, Emmett PH, Teller E. Adsorption of gases in multimolecular layers. J Am Chem Soc 1938;60:309–19.
[59] Barrett EP, Joyner LG, Halenda PP. The determination of pore volume and area distributions in porous substances. Computations from nitrogen isotherms. J Amer Chem Soc 1951;73:373–80.
[60] Chen Ch-M, Dai Y-M, Huang JG, Jehng J-M. Intermetallic catalyst for carbon nanotubes (CNTs) growth by thermal chemical vapor deposition method. Carbon 2006;44:1808–20.
[61] Raemy A, Schweizer TF. Thermal behaviour of carbohydrates studied by heat flow calorimetry. J Therm Anal 1983;28:95–108.
[62] Dresselhaus MS, Dresselhaus G, Jorio A, Souza Filho AG, Saito R. Raman spectroscopy of isolated single wall carbon nanotubes. Carbon 2001;40:2043–61.
[63] Roy D, Chhowalla M, Wang H, Sano N, Alexandrou I, Clyne TW, et al. Characterisation of carbon nano-onions using Raman spectroscopy. Chem Phys Lett 2003;373:52–6.
[64] Obratzova ED, Fujii M, Hayashi S, Kuznetzov VL, Butenko YV. Raman identification of onion-like *carbon*. Carbon 1998;36:821–6.
[65] Tuinstra F, Koenig JL. Raman spectrum of graphite. J Chem Phys 1970;53:1126–30.
[66] Al-Jishi R, Dresselhaus G. Lattice-dynamical model for graphite. Phys Rev B 1982;26:4514–22.
[67] Nemanich RJ, Solin SA. First- and second-order Raman scattering from finite-size crystals of graphite. Phys Rev B 1979;20:392–401.
[68] Jorio A, Dresselhaus G, Dresselhaus MS, Souza M, Dantas MSS, Pimenta MA, et al. Polarized Raman study of single-wall semiconducting carbon nanotubes. Phys Rev Lett 2000;85:2617–20.
[69] Solin SA, Ramdas AK. Characterization of diamond films by Raman spectroscopy. Phys Rev B 1970;1:1687–98.
[70] Ferrari AC, Meyer JC, Scardaci V, Casiraghi C, Lazzeri M, Mauri F, et al. Raman spectrum of graphene and graphene layers. Phys Rev Lett 2006;97:187401–4.
[71] Lucchese MM, Stavale F, Martins Ferreira EH, Vilani C, Moutinho MVO, Capaz RB, et al. Quantifying ion-induced defects and raman relaxation length in graphene. Carbon 2010;48:1592–7.
[72] Cancado LG, Takai K, Enoki T, Endo M, Kim YA, Mizusaki H, et al. General equation for the determination of the crystallite size La of nanographite by Raman spectroscopy. Appl Phys Lett 2006;88:163106–16.
[73] Tuinstra F, Koenig JL. Raman spectrum of graphite. J Chem Phys 1970;53:1126–30.
[74] Song F, Echegoyen L. In situ spectroelectrochemistry and electrochemical quartz crystal microbalance (EQCM) charaterization of C_{60} embedded in a tetraoctylammonium bromide film in aqueous solution. J Phys Chem B 2003;107(24):5844–50.
[75] Watanabe K, Komatsu M, Niidome Y, Murata M, Murata Y, Komatsu K, et al. Electrochemistry of an open-cage fullerene embedded in a film of hydrophobic ammonium ion on an electrode. J Phys Chem C 2007;111:6500–4.
[76] Plonska-Brzezinska ME, Palkar A, Winkler K, Echegoyen L. Electrochemical properties of small carbon nano-onion films. Electrochem Solid-State Lett 2010;13(4):K35–8.
[77] Kinoshita K, Bett JAS. Influence of electrochemical treatment in phosphoric acid on the wettability of carbons. Carbon 1975;13:405–9.
[78] Fernandez-Prini R. In: Covington AK, Dickson T, editors. Physical chemistry of organic solvent systems. New York: Plenum Press; 1973.